

**Ka-Band Propagation Studies Using the ACTS
Propagation Terminal and the CSU- CHILL
Multiparameter Radar**

(A Two Year Report)

Experiment ers

Colorado State University
Department of Electrical Engineering
Ft. Collins, CO 80523

Investigators

V. N. Bringi, Professor
John Beaver

**NASA Propagation Experimenters Meeting
(NAPEX XX)
June 4-6, 1996
Fairbanks, Alaska**

Contents

1	Introduction.	2
2	Statistical Attenuation Analysis at Ka-Band	3
2.1	CSU-ACTS Propagation Data	4
2.2	Description of Statistical Quantities	5
3	CSU-CHILL Polarimetric Radar Data	7
3.1	Radar Descriptio	7
3.2	Radar Observables	7
3.3	Attenuation Estimates	10
4	Concurrent CSU-APT and CSU-CHILL Measurements	12
4.1	Attenuation Events	13
4.2	Attenuation Estimates	19
5	Conclusions	27
A	Statistical Results for Analysis Period of December 1, 1993 through November 30, 1995	28
A.1	Monthly Analysis for December 1, 1993 through November 30,1994	29
A.2	Annual Results for December 1, 1993 through November 30, 1994	84
A.3	Monthly Anal ysis for December 1, 1994 through November 30,1995	93
A.4	Annual Results for December 1, 1994 through November 30, 1995	150
A.5	Monthly and Annual CDF Comparisons for 1994 and 1995. .	159

1 Introduction

There has been an increased interest in utilizing the Ka-band frequency spectrum from industry. Currently several industry leaders are in the process of setting up satellite communication systems that operate at the Ka-band frequencies or already have systems in place. The increased interest in operating such systems at the Ka-band frequencies is mainly due to overcrowding of the current spectrums at C- and Ku-bands. Of course, other benefits exist such as an increase in data transmission rates, an increase in the amount of information that is being transmitted and smaller Earth receiving stations which leads to greater mobility. However, along with the benefits there are some disadvantages of operating at these frequencies, such as increased attenuation effects due to the atmospheric conditions.

One of the attractive features that led to the use of C- and Ku- bands for satellite communications was the low susceptibility to attenuation effects caused by rain or clouds. The larger wavelengths are minimally affected by the atmospheric conditions. The Ka- band frequencies, however are very susceptible to weather-related events. Rain, clouds and even gaseous absorption by oxygen and water vapor can adversely affect the signal and must be considered. Rain can easily produce 20 to 30 dB of attenuation at the Ka- band frequencies. For space-to-Earth links with low elevation angles, tropospheric scintillations can also cause appreciable attenuation. Therefore, before being used commercially, propagation effects at Ka- band must be studied.

One of the first experimental communication satellites using Ka-band technology is the National Aeronautics and Space Administration's (NASA) Advanced Communications Technology Satellite (ACTS). In September 1993, ACTS was deployed into a geostationary orbit near 100° W longitude by the space shuttle Discovery. The ACTS system supports both communication and propagation experiments at the 20/30 GHz frequency bands. The propagation experiment involves multi-year attenuation measurements along the satellite- Earth slant path.

Colorado State University (CSU) and six other sites across the United States and Canada are conducting the propagation studies. Each site is equipped with the ACTS propagation terminal (APT). The APT's were designed and built by Virginia Tech's Satellite Communications Group [8] and

are receive only Earth stations. Each site is located in a different climatic zone, with CSU in the newly designated B2 climate zone. In addition to the Colorado site, other propagation sites include British Columbia, Alaska, New Mexico, Oklahoma, Florida and Maryland.

The overall goal for the propagation experiment is to obtain high quality attenuation measurements in order to construct a data base so that the attenuation effects at Ka-band frequencies can be statistically characterized. This statistical analysis is to be done on a monthly and annual basis. The monthly resolution makes this study a unique one as most attenuation statistics available today are on an annual basis. This is also true for most of the statistical models available to date.

In addition to the overall goal, each site is applying its own expertise to secondary studies. CSU's contribution is the application of polarimetric radar data for attenuation prediction. Radar data taken by the CSU- CHILL, fully polarimetric, multiparameter Doppler radar is used to gain a greater understanding of the microphysical processes that are responsible for Ka-band attenuation that occurs along the ACTS slant path. Radar data are used to initialize a radar-- based attenuation model that has been developed for this research.

This paper outlines the methods used to obtain the stated goals and presents results from the first two years of data collection. A description of the statistical analysis done at CSU for the first two years of the experiment are presented in Section 2. The statistics presented include cumulative distributions for attenuation measurements, attenuation ratio data, fade and non- fade duration analysis and fade slope computations. Section 3 gives a brief description of the CSU- CHILL radar, along with definitions of several radar observable that will be used in this study. A description of the attenuation model developed for this research is also presented in this chapter. Section 4 presents three case studies for which concurrent measurements from the CSU-APT and CSU-CHILL radar were available. Results using the attenuation model are given and analyzed. Finally, Section 5 presents some conclusions that were obtained from this research.

2 Statistical Attenuation Analysis at Ka- Band

A description of the propagation data and the statistical analysis completed on the measured CSU-APT data is presented in this chapter. The results are presented as primary and secondary statistics, as defined by Virginia

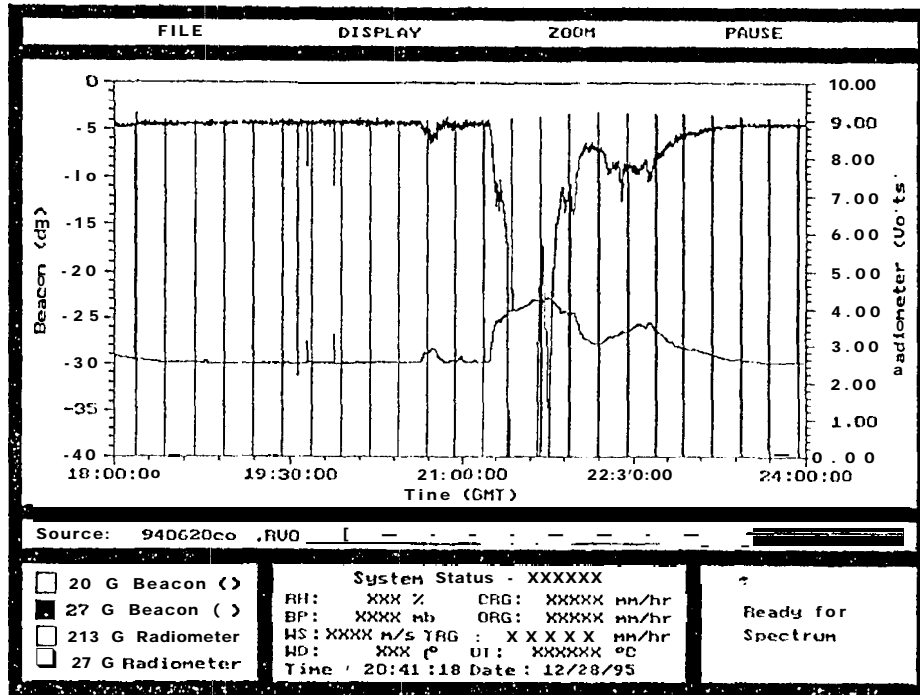


Figure 1: CSU-APT raw propagation data for June 20, 1994 rain event.

Tech during the Olympus propagation experiment [7]. The analysis period is for December 1, 1993 through November 30, 1995. Attenuation statistics are computed for a monthly and annual basis.

2.1 CSU-ACTS Propagation Data

Before a statistical analysis is performed on the data, it must be preprocessed. An example of a raw data set is shown in Figure 1, for the 27 GHz beacon and radiometer channels. The data is taken from June 20, 1994. The raw data is contaminated from various sources; a few will be briefly described here. The periodic dropouts in the beacon data that occur every 15 minutes are points where automatic calibrations occur. The beacon and radiometer data are assigned special values during these calibrations and should not be included in the final attenuation data. Dropouts in the beacon level that are not weather related, such as during maintenance periods, also should not be included in the data. Other factors that may affect the raw data signal include solar and lunar eclipses, satellite maneuvering and diurnal effects.

To obtain “clean” attenuation data, the raw data is processed through software that was developed by Crane and Westenhaver [4]. The prepro-

cessing software automatically marks data bad during calibration periods, eclipse periods and periods of non-therms] events (such as when the Sun is aligned along the propagation path). Diurnal effects are also automatically removed by the preprocessing code. For effects that cannot be automatically determined, such as maintenance periods or the occasional beacon dropout, the data can be manually marked as bad. Finally, system calibration is also incorporated into the preprocessing code [4]. The final output from the software is calibrated attenuation data, with all bad data points removed. Parameters that are used in tile statistical analysis are radiometrically derived attenuation (ARD) and attenuation with respect to free space (AFS)[7].

2.2 Description of Statistical Quantities

The statistical analysis presented by Virginia Tech from the Olympus propagation program, was separated into two types - primary and secondary statistics [7]. The primary statistics include cumulative distribution functions of the AFS and ARD data, as well as attenuation ratio data between two frequencies. A common time base is used for all the primary statistics computed so that a valid comparison is made between the quantities of interest. Secondary statistics include fade durations, non-fade durations and fade slope data. For these types of statistics a common time base is not used. The methods used to compute primary statistics is discussed first.

Cumulative distribution functions (CDF) are computed for ARD and AFS data at both 20 and 27 GHz. The data are binned from -3.0 to 30 dB in increments of 0.1 dB. The data are presented as a percentage of time exceeded versus attenuation level. Data used to construct the CDF plots, are taken from the 1-Hz samples of preprocessed data, with no average applied to the data.

Attenuation ratio (RA) data are presented here in the form of a percentage of time exceeded versus dB ratio and dB level exceeded versus dB ratio. First the data are averaged by applying a 30- second moving block average to remove any scintillation effects. The attenuation ratio is then obtained by dividing the 27 GHz AFS with the base frequency of 20 GHz AFS (both values are in dB). The RA values are binned from 0.0 to 10.0 in increments of 0.05 for all base attenuation levels greater than 1 dB. The RA data are also binned for different base dB levels, the base dB level ranges from 0 to 30 dB in increments of 1 dB. RA versus dB level exceeded is used to determine when an RA value, for a specific dB level, exceeds a specific

value for a certain amount of time. The exceedance curves are given for 1 %, 10%, 50%, 90% and 99% of the time.

While the primary statistics are used mainly for direct comparison of data between two frequencies or for scaling information, the secondary statistics are used more to look at the individual characteristics at each frequency. They contain information regarding fade duration, inter-fade duration and fade slope characteristics. Fade duration data is discussed first.

Fade duration (FD) is defined as the amount of time that the attenuation level (AFS) exceeds a specified threshold, T [7]

$$FD(\overline{AFS}_T) = t_2 - t_1 \quad (1)$$

where

$$\overline{AFS} \geq \overline{AFS}_T \quad \text{for } t_1 < t < t_2 \quad (2)$$

The bar indicates that a moving average has been applied to the data. In this case a 30-second moving average is used before the fade duration computations were done. Similarly the non-fade or inter-fade duration (IFD) is defined as

$$IFD(\overline{AFS}_T) = t_2 - t_1 \quad (3)$$

where

$$\overline{AFS} \leq \overline{AFS}_T \quad \text{for } t_1 < t < t_2 \quad (4)$$

Data are presented for the number of fade events for a given threshold level versus a specified fade duration. The percentage of time for all fades for a given threshold level versus a specific fade duration is also computed. The threshold level ranges from 0 to 30 db in increments of 1 dB, while the fade duration bins are 0-1, 1-2, 2-3, 3-5, 5-6, 6-10, 10-15, 15-18, 18-20, 20-30, 30-60, 60-120, 120-180, 180-300, 300-600, 600-1200, 1200-1800 and 1800-3600 seconds. Non-fade duration data is computed in the same manner.

Finally, fade slope (FS) information is obtained. The fade slope is computed after applying a 10 second moving average on the AFS data to remove signal fluctuations due to scintillation effects. It is defined only if the attenuation level crosses a specified threshold and remains either larger or smaller than the threshold for more than 10 seconds. The fade slope for a given threshold crossing is defined as [7]

$$FS_i = \frac{\overline{AFS}_{i+5} - \overline{AFS}_{i-5}}{10} \quad (5)$$

where \overline{AFS} is given as

$$\overline{AFS}_k = \frac{1}{10} \sum_{j=k-4}^{j=k+5} AFS_j \quad (6)$$

and i is the index value when the attenuation crosses a specified threshold. The threshold values range from 0 to 30 dB in increments of 1 dB, while the fade slope values are binned from -1.25 to 1.25 dB/sec in increments of 0.05 dB/sec.

Primary and secondary statistics are computed on a monthly basis and annually for the period of December 1, 1993 to November 30, 1995. Results obtained at CSU for the two year period are given in Appendix A.

3 CSU-CHILL Polarimetric Radar Data

3.1 Radar Description

The CHILL radar has an historic past as it was one of the first radars to utilize polarization diversity. The radar was originally designed and constructed jointly by the University of Chicago and the Illinois Water Survey under the guidance of Mueller and Atlas [2]. In 1990, the CHILL radar was moved to its present location outside of Greeley, Colorado and is now used exclusively as a research radar operated by CSU under the sponsorship of the National Science Foundation. It is a fully polarimetric S-band radar that can alternately send two orthogonally polarized signals and simultaneously receive the co- and cross-polarized signals. With recent upgrades made to the radar it is now ranks as one of the top radars of its kind. A summary of the system characteristics are given in Table 1

3.2 Radar Observable

The CSU-CHILL radar transmits and receives both horizontal and vertical polarizations. Being able to measure both the copolar and cross-polar returns allows measurements of such quantities as the horizontal reflectivity (Z_H), differential reflectivity (Z_{DR}), the specific differential phase between the H and V copolar signals (K_{DP}) and the differential propagation phase shift (ϕ_{DP}). The correlation coefficient between the two copolar signals (ρ_{HV}) and the linear depolarization ratio (LDR) are also measured. The radar observables can be defined in terms of the forward and back scattering amplitudes and the raindrop size distribution. The first subscript of the

Table 1: System Characteristics of the CSU-CHILL Radar

Antenna	
type:	fully steerable, prime focus parabolic reflector
size:	8.5 m
feed:	scalar horn
3 dB beamwidth:	1.0°
directivity :	45 dB
sidelobe level (any #-plane):	≤ -27 dB
cross-pol. level (any @-plane):	≤ -30 dB
polarization radiated:	Horizontal or Vertical
Transmitter	
type:	klystron, modernized FJ 'S- 18
wavelength:	10.7 cm
peak Power:	700- 1000 kW
pulse width:	steps of 0.1 μs up to a max. of 1 μs
PRT:	800 - 2500 μs
max. unambigu. range:	375 km
max. unambigu. velocity:	±34.3 m/s
Receiver	
noise figure:	0.7 dB
noise power:	-- 114 dBm
typical bandwidth:	750 kHz
transfer function:	linear
dynamic range:	90 dB, O -60 dBIAGC in 12 dB steps
Data Acquisition	
signal processor:	SP20 made by Lassen Research
number of range gates:	64-2048
range gate spacing:	0.2 μs or 1 μs
sampling rate/avg. option:	under micro-code control
video digitizer:	12-bit, in the SP20 input card for I, Q and logP
time series capability:	up to 150 range gates.
Variables Available	
<ul style="list-style-type: none"> ● Reflectivity at H polarization (Z_h) ● Differential Reflectivity (Z_{dr}) ● Mean Doppler velocity (\bar{v}) and Spectral Width (σ_v) ● Differential Phase between H and V states (Ψ_{dp}) ● Copolar Correlation Coefficient ($\rho_{hv}(0)$) ● Linear Depolarization Ratio (LDR) ● Doppler Spectra from FFT processing ● I, Q and logP for every pulse in time series mode (up to 150 gates) 	

polarization states given in the following equations refers to the received polarization state, while the second subscript refers to the transmitted polarization state. The horizontal and vertical reflectivity are defined by

$$Z_{HH,VV} = \frac{\lambda^4}{\pi^5 |K|^2} \int \sigma_{HH,VV}(D) N(D) dD, \quad \text{mm}^6 \text{m}^{-3}, \quad (7)$$

where $\sigma_{HH,VV}(D)$ are the copolar radar cross sections at the horizontal and vertical polarizations, $|K| = (\epsilon_r - 1) / (\epsilon_r + 2)$, ϵ_r is the dielectric constant of water and λ is the wavelength [5]. Differential reflectivity is defined as

$$Z_{DR} = 10 \log \left(\frac{Z_{HH}}{Z_{VV}} \right) \quad \text{dB} \quad (8)$$

Defining f_{HH} and f_{VV} as the forward scattering amplitudes of the H and V polarized waves, the specific differential phase is given as

$$K_{DP} = \frac{180\lambda}{\pi} \int \text{Re} [f_{HH}(D) - f_{VV}(D)] N(D) dD \quad (\text{deg/km}) \quad (9)$$

Then ϕ_{DP} is defined as

$$\phi_{DP} = \int_{r_1}^{r_2} 2K_{DP}(r) dr \quad (\text{deg}) \quad (10)$$

where ϕ_{DP} is the two-way differential phase between range locations, r_1 and r_2 . If the backscatter amplitudes for the horizontal and vertical polarizations are defined as S_{HH} and S_{VV} , then the cross-correlation coefficient is given as

$$\rho_{HV} = \frac{\int S_{HH}(D) S_{VV}^*(D) N(D) dD}{\left\{ \left[\int |S_{HH}|^2 N(D) dD \right] \left[\int |S_{VV}|^2 N(D) dD \right] \right\}^{1/2}} \quad (11)$$

The linear depolarization ratio can also be defined in terms of the backscatter amplitudes

$$LDR_{VH} = 10 \log \frac{|S_{HV}|^2}{|S_{HH}|^2} \quad (\text{dB}) \quad (12)$$

The variable $N(D)$ is the raindrop size distribution in equations 7-12 and is the number of raindrops per unit volume per unit size interval D to $D + \delta D$, where D refers to the equivalent spherical diameter [6].

Each polarimetric parameter provides information about the type of particles present in a given radar range resolution volume. For instance, information regarding a particle's shape can be obtained from the differential reflectivity, while information about a particle's orientation can be

obtained from the linear depolarization ratio. Specific differential phase is sensitive only to non-spherical particles such as oblate raindrops or aligned ice crystals. While each of these parameters provide information on their own, looking at a combination of polarimetric parameters can give an even greater insight to what is occurring; in a particular storm cell. For example, reflectivity and differential reflectivity used together can be a good indicator to determine if a range resolution volume contains hail particles. Typically, if hail is present the reflectivity values tend to be high, while the tumbling nature of hail stones results in low values for differential reflectivity. This is just one of many examples of how polarimetric parameters can be used in describing the internal structure of storm events.

3.3 Attenuation Estimates

To obtain K-band attenuation estimates from S-band reflectivity data, simulations were obtained by varying the parameters of a given drop size distribution (11 D). Using a Mie solution for spherical water particles, propagation variables such as K- band attenuation and S- band reflectivity were computed using a wide range of DSD parameters. In this case a gamma DSD was used

$$N(D) = N_0 D^m e^{-\gamma D} \quad (13)$$

where

$$\gamma = \frac{3.67 + m}{D_0} \quad (14)$$

and $N(D)$, given in mm^{-3} , is the number of drops per unit volume per unit size interval, D is the equivalent drop size diameter in mm, N_0 is given in mm^{-3} , D_0 is the median drop size in mm and m is the shape factor. The DSD triplets (N_0 , D_0 , m) are varied as follows: $100 \leq N_0 \leq 50000$, $1 < D_0 \leq 4$ and $0 \leq m \leq 5$. Results of the simulation are shown in Figure 2. Each point on the scatter plot represents K-band attenuation and S- band reflectivity for a given DSD triplet. The entire range of triplets are representative of actual drop size distributions for a wide variety of rainfall events [1].

The S- band reflectivity/K-band attenuation curves are obtained by applying a power function fit to the simulated data. The equation that relates S-band reflectivity to K--band attenuation is given by

$$AK = a \left(10^{Z_S/10} \right)^b \quad (15)$$

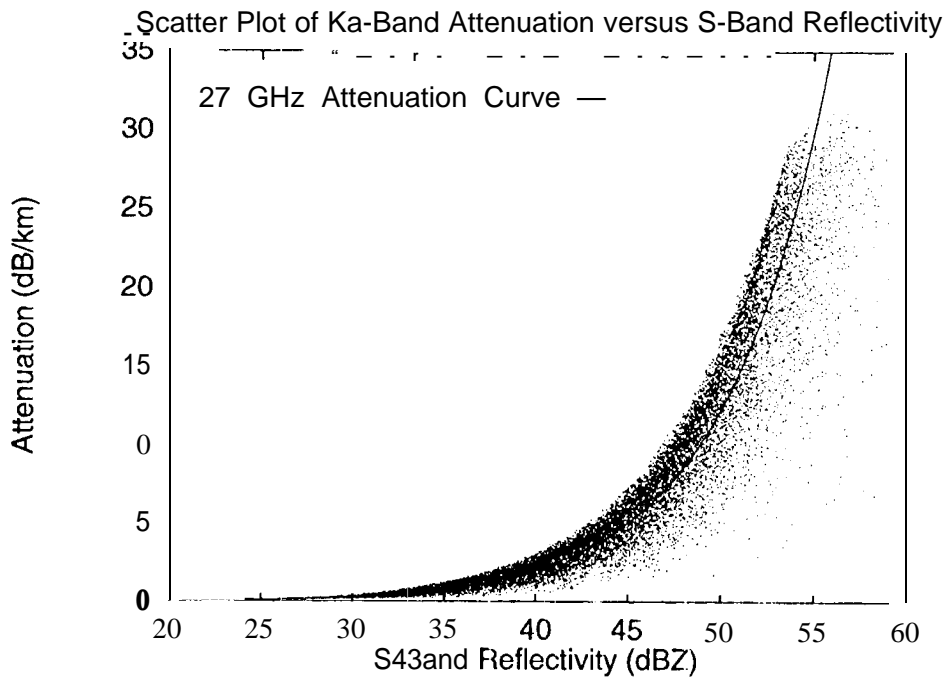
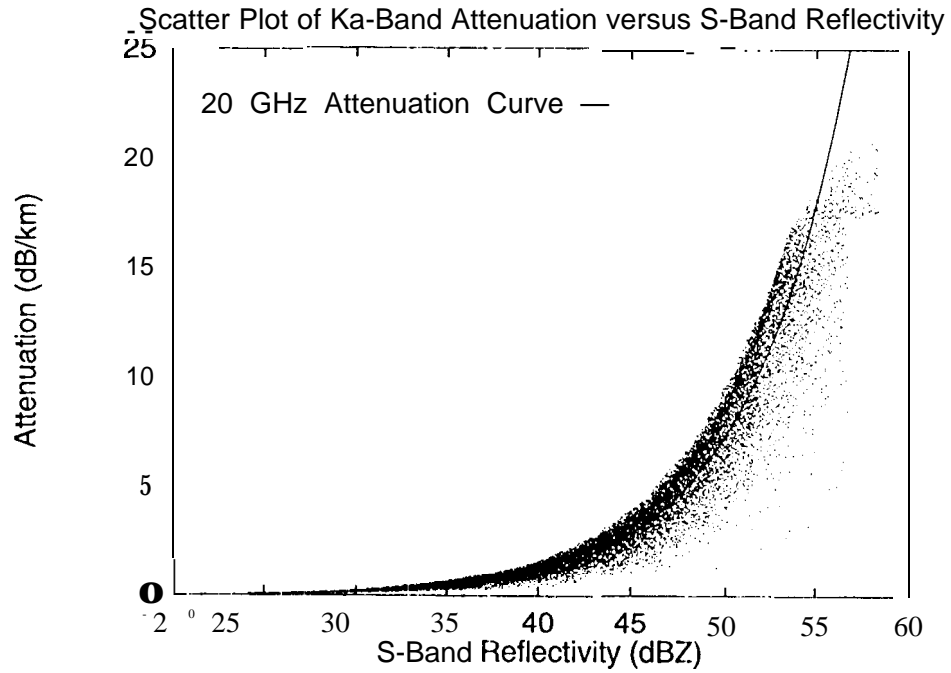


Figure 2: Attenuation for 20 and 27 GHz versus reflectivity at 3 GHz, obtained using a Mie solution for spherical particles.

Table 2: Values for a and b given in equation 15

Frequency	a	b
20 GHz	7.1×10^{-4}	8.0×10^{-1}
27 GHz	1.7×10^{-3}	7.7×10^{-1}

where AK is K-band attenuation and Z_S (in dB) is S-band reflectivity. Values for a and b are given in Table 2.

Simulations were also conducted using a two-layered Mie solution. Several scatter plots were obtained by simulating water coated ice particles and varying the fraction of ice to water. The gamma DSD triplets were varied as before. Particles that were simulated ranged from spheres with small ice cores and a thick layer of water to spheres with large ice cores and a very thin layer of water. The derived attenuation curves in each case were almost identical to those shown in Figure 3.3. Any variations that were noted fell well within the scatter of the DSD parameters for pure water.

Attenuation curves relating K-band attenuation versus S-band specific differential phase, KDP , were also derived. The T-matrix solution was used to obtain the scattering amplitudes for oblate raindrops ranging in size from 1-8 mm. S-band KDP and specific attenuation at Ka-band were then computed from the Mueller matrix, averaged over an exponential DSD ($m = 0$ in the gamma DSD). The attenuation curves, shown in Figure 3, were obtained by varying the DSD parameter D_0 , while N_0 was fixed at $8000 \text{ mm}^{-1} \text{ m}^{-3}$.

4 Concurrent CSU-APT and CSU-CHILL Measurements

The Colorado Front range experiences a variety of weather events throughout the year, ranging from upslope rain conditions to winter storms producing wet snow and sleet, to widespread convective episodes in the late summer. Three such events are presented in this section. These include one stratiform event with a well defined “bright band”, where there was light-to-moderate precipitation uniformly covering a large area. Also presented are two convective cases, which are highly variable in nature and more localized

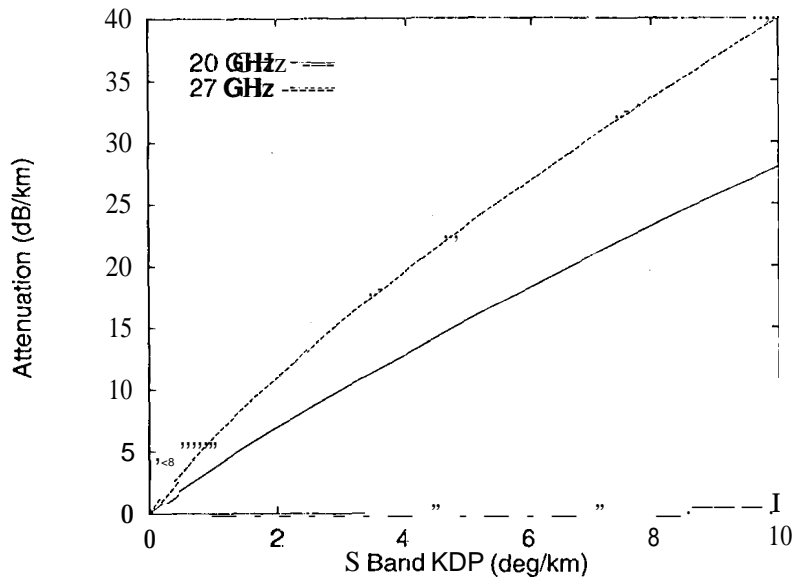


Figure 3: Attenuation for 20 and 27 GHz versus specific differential phase at 3 GHz, obtained via T-matrix and Mueller matrix solutions.

to a particular region.

The events are presented in the order of occurrence and include a June 20, 1994 convective event, a May 18, 1995 collective event and finally, a June 18, 1995 stratiform event. For these three events many radar scans are taken along the ACTS propagation path during the course of the attenuation event. The CSU-APT is co-located at the CSU-CHILL radar site. The APT azimuthal position is 172° from North and its elevation is 43° . This section first gives a description of the concurrent measurements obtained by the CSU-APT and the CSU-CHILL radar and then presents the results obtained using the S-band reflectivity /Ka-band attenuation model presented in Section 3.

4.1 Attenuation Events

A strong convective attenuation event occurred on June 20, 1994 causing a signal loss at 27 GHz for approximately 15 minutes. The 20 GHz signal bounced in and out of lock several times, but for only very short durations. Figure 4 shows the measured APT data for both the 20 and 27 GHz channels. Attenuation levels actually reached the 30 dB level at both frequencies

Attenuation Due to Rain Event

6/20/94 ACTS Propagation Data (CO)

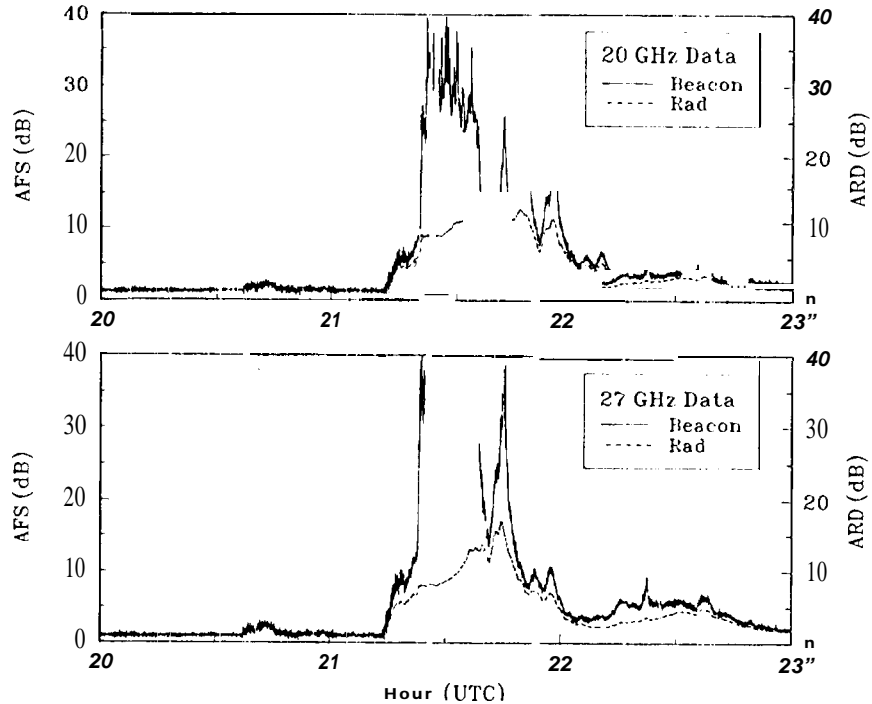


Figure 4: CSU-APT attenuation measurements for the June 20, 1994 convective case.

before the signal began to cut in and out. The event started at approximately 21:14 UTC, with large attenuation present at both frequencies until 22:01 UTC. Concurrent radar data were also taken for the June 20 rain event. Figure 5 shows an RHI plot taken at 21:32 UTC. Reflectivity values along the propagation path are on the order of 45 dBZ, at 6.5 km Z_H reaches a maximum of 54 dBZ. Values of Z_{DR} are on the order of 0.3 to 0.5 dB along the propagation path. In the area of peak reflectivity the Z_{DR} values are approximately 0.5 to 0.8 dB. These low values of Z_{DR} combined with the high reflectivity values gives an indication that there may be tumbling hailstones in that particular region. Panel 3 shows a dip in the cross correlation coefficient in the region of low Z_{DR} and high Z_H , while along the rest of the propagation path it is 0.98 or greater. There are also measurable values of specific differential phase, KDP , at 6.5 km, as shown in Panel 4 of Figure 5. Values of KDP along the slant path were approximately 0.5 to 0.6 deg/km. The presence of KDP and a minimum in the correlation coefficient at 6.5

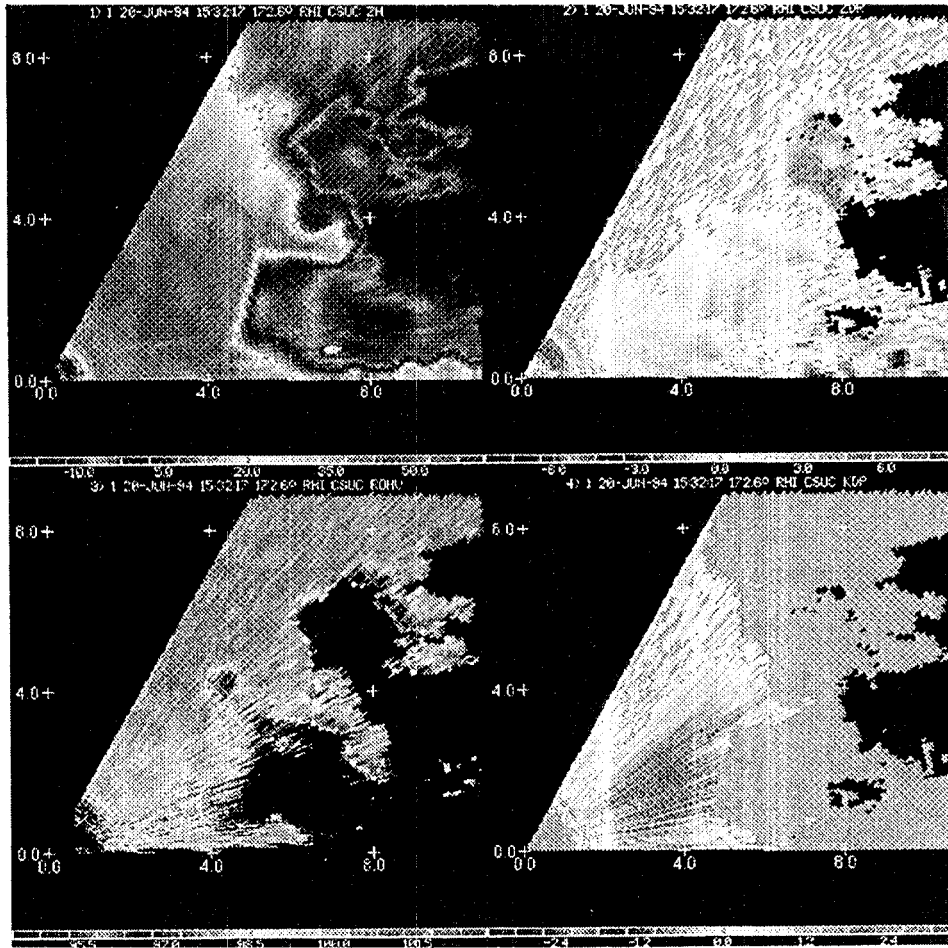


Figure .5: RH1 scan for the June 20, 1994 convective case. The scan is taken along the radial of the ACTS propagation path. The CSU-APT elevation angle is 43° . The radar is located at the origin with the height given in km along the y-axis. Distance away from the radar along the 172° azimuthal angle is given in km along the x-axis. Horizontal reflectivity, Z_{HH} (dBZ), is shown in the upper left panel. Differential reflectivity, Z_{DR} (dB), is shown in the upper right panel. The cross correlation coefficient, ρ_{HV} (given as a percentage), is shown in the lower left panel. Specific differential phase, K_{DP} (deg/km), is shown in the lower right panel.

ACTS Data - Convective Case

5/18/95 ACTS Propagation Data (CO)

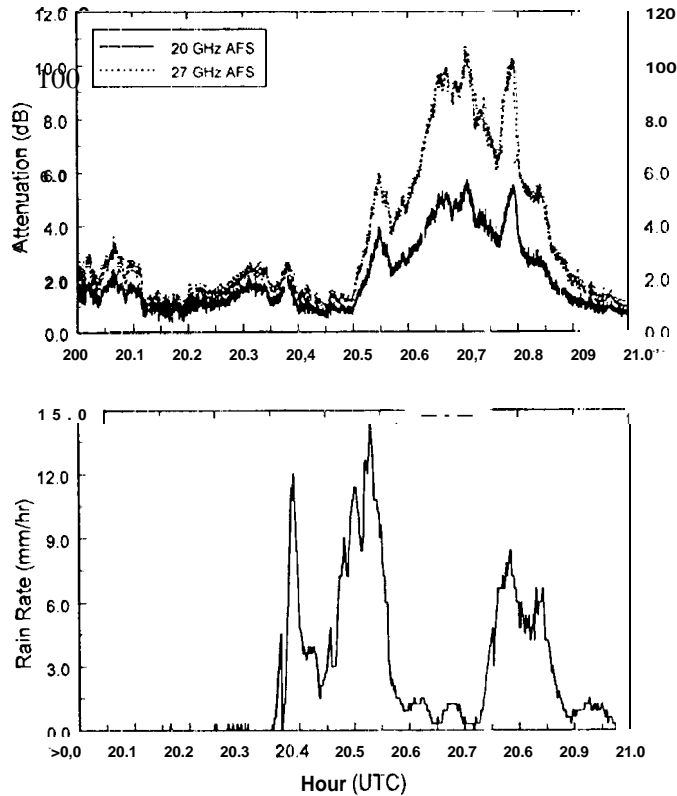


Figure 6: CSU-APT beacon attenuation measurements and the corresponding rain rate for the May 18, 1995 convective case.

km, is an indication that this region is an area of mixed phase. The region consists of tumbling hailstones, along with water coated ice particles, that can produce pure water droplets through a shedding effect. This region of mixed phase occurs right along the along the ACTS propagation path.

A second, weaker, convective event was observed on May 18, 1995. The CSU-APT measured attenuation, along with corresponding rain rates, is shown in Figure 6. The APT measured attenuation reaches a maximum of 10-11 dB for the 27 GHz signal and 5 dB for the 20 GHz signal. The event began at 20:30 UTC and lasted until 20:56 UTC. A total of 72 radar scans taken directly along the slant path between 20:32 to 20:56 UTC were available for this event. A sample of the radar data measured during this event is shown in Figure 7, again as an RHI plot. Panel 1 shows that the reflectivity values range from 15 dBZ to 40 dBZ along the propagation path. Z_{DR} had peak values of 0.7-0.9 dB, while high values of ρ_{HV} is indicative to that of rain. Larger values of KDP , shown in the Panel 4, are mostly present at the lower elevation angles farther out in range from the radar

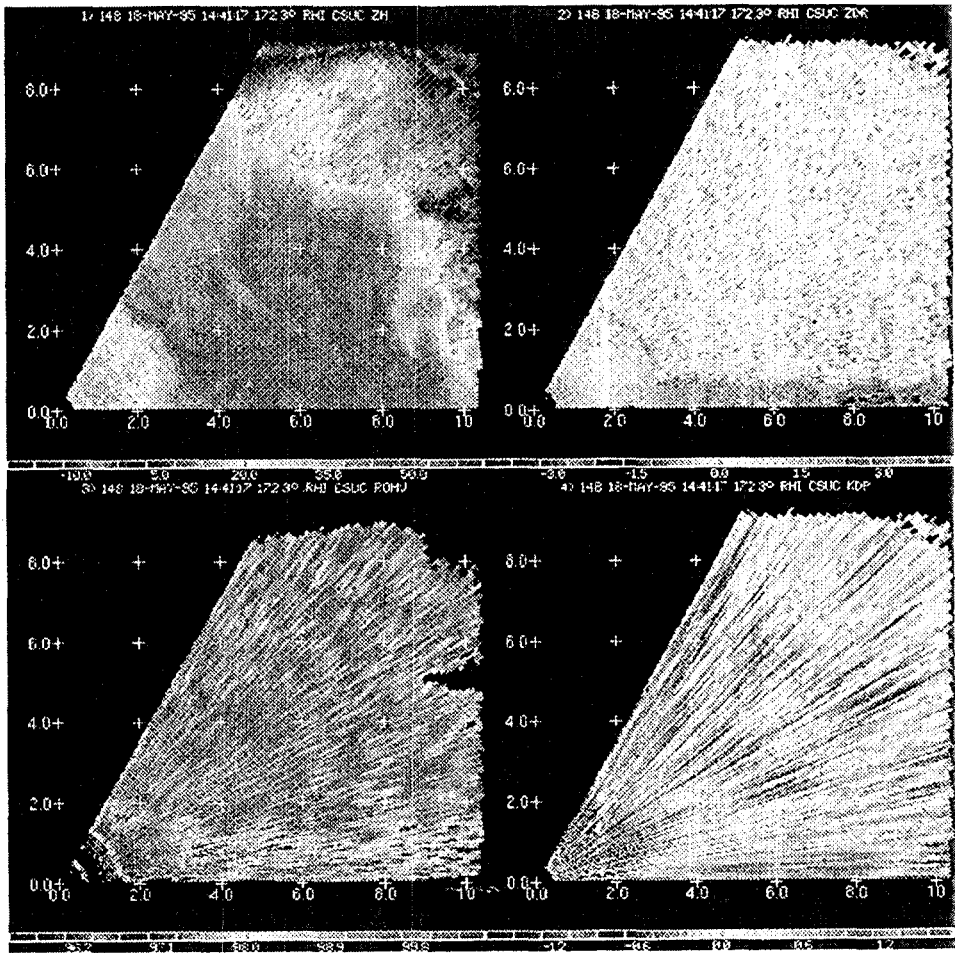


Figure 7: RHI scan for the May 18, 1995 convective case. The scan is taken along the radial of the ACTS propagation path. The CSU-APT' elevation angle is 43° . The radar is located at the origin with the height given in km along the y- axis. Distance away from the radar along the 172° azimuthal angle is given in km along the x- axis. Horizontal reflectivity, Z_{HH} (dBZ), is shown in the upper left panel. Differential reflectivity, Z_{DR} (dB), is shown in the upper right panel. The cross correlation coefficient, ρ_{HV} (given as a percentage), is shown in the lower left panel. Specific differential phase, K_{DP} (deg/km), is shown in the lower right panel].

ACTS Data - Stratiform Case

6/18/95 ACTS Propagation Data (CO)

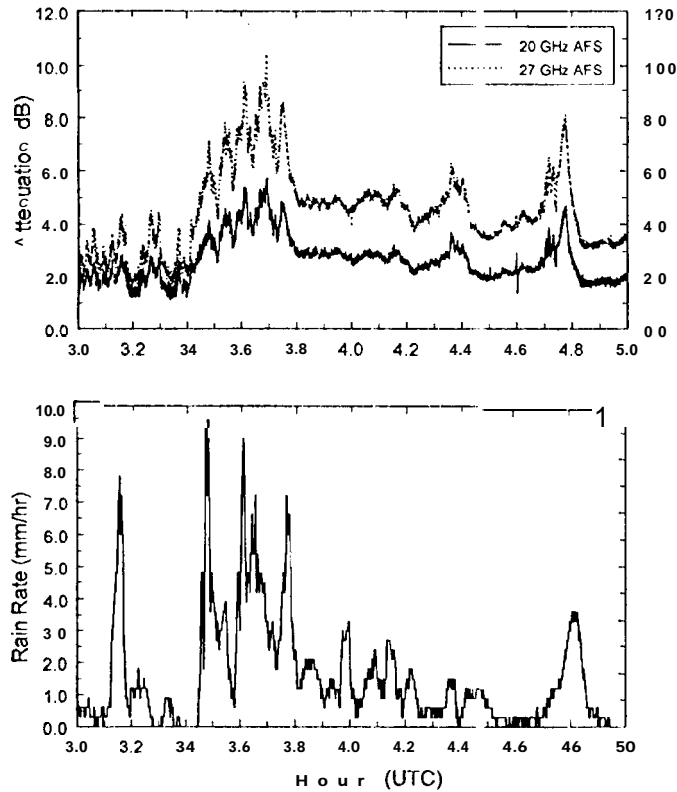


Figure 8: CSU--A PT beacon attenuation measurements and the corresponding rain rate for the June 18, 1995 stratiform case.

and not along the slant path. The radar data, along with the rain rate data obtained at the site, indicate that a very light rain has occurred at the site, while most of the attenuation is due to precipitation farther out along the slant path.

The last case to be examined is a stratiform event that occurred on June 18, 1995. As shown in Figure 8, this is actually a stratiform case with some embedded convection in the initial stages of the event. Peak values of attenuation measured by the APT were around 10 dB for the 27 GHz signal and 5 dB for the 20 GHz signal, during the embedded convective part of the event. In the more stable stratiform region the attenuation was approximately 5 and 3 dB, for the 27 and 20 GHz signals respectively. The rain rates for this event are also given, with peak rates of only 6-9 mm/hr during the portion of the event with embedded convection and 1-3 mm/hr during the stratiform only time of the event. For this event, 120 radar scans were taken along the propagation path.

An RHI plot taken at 4:21 UTC is shown in Figure 9. The measured hor-

horizontal reflectivity was about 45 dBZ in the region of the bright band, while values of 30 dBZ are seen along the propagation path below the reflectivity bright band. The height of the reflectivity bright band is approximately 2.45 km. Z_{DR} values in the melting layer were approximately 1.0- 1.5 dB, with values of 0.5--0.8 dB below the melting layer. The ρ_{HV} data exhibits the typical decrease in magnitude in the melting region, with values dropping to 0.93. The final radar parameter given in this RHI plot is the linear depolarization ratio (LDR) and it has values up to -18 dB in the melting layer.

The next step in the analysis process is to use the radar information as input to the propagation model on a case-by-case basis. Results using the S-band reflectivity/Ka-band attenuation model are presented in the next section for the three case studies.

4.2 Attenuation Estimates

Attenuation estimates have been computed using the S-band reflectivity /Ka-band attenuation model derived in Section 3.3. Only the reflectivity values have been used to model the cases described in the previous section (KDP estimates were used in the June 20, 1994 convective case), while the polarimetric parameters Z_{DR} , KDP and ρ_{HV} were used to determine the length of the attenuation path. These polarimetric parameters are dependent on the elevation angle of the radar, therefore a correction factor is used to obtain values of Z_{DR} and KDP for an elevation angle of 0° . The corrected values are used as input to the attenuation model.

Radar scans were taken directly along the ACTS propagation path with a range resolution of 150 m. Reflectivity data at 3 GHz were taken at the 150 m increments and used to determine the corresponding 20 and 27 GHz attenuation estimates from the attenuation curves given in Figure 2. The Ka-band attenuation estimates were then multiplied by the appropriate distance along the propagation path.

For the June 20, 1994 convective case, 43 radar scans were taken throughout the duration of the event. Ka-band attenuation estimates were derived from S-band reflectivity data using the procedure described above. For this particular event S-band KDP data are also used to derive Ka-band attenuation estimates. The results are shown in Figure 10

As seen in Figure 10, the CSU-CHILL reflectivity based attenuation estimates follow the attenuation measurements obtained from the APT very closely. The maximum difference is about 5 db, while for the most part the

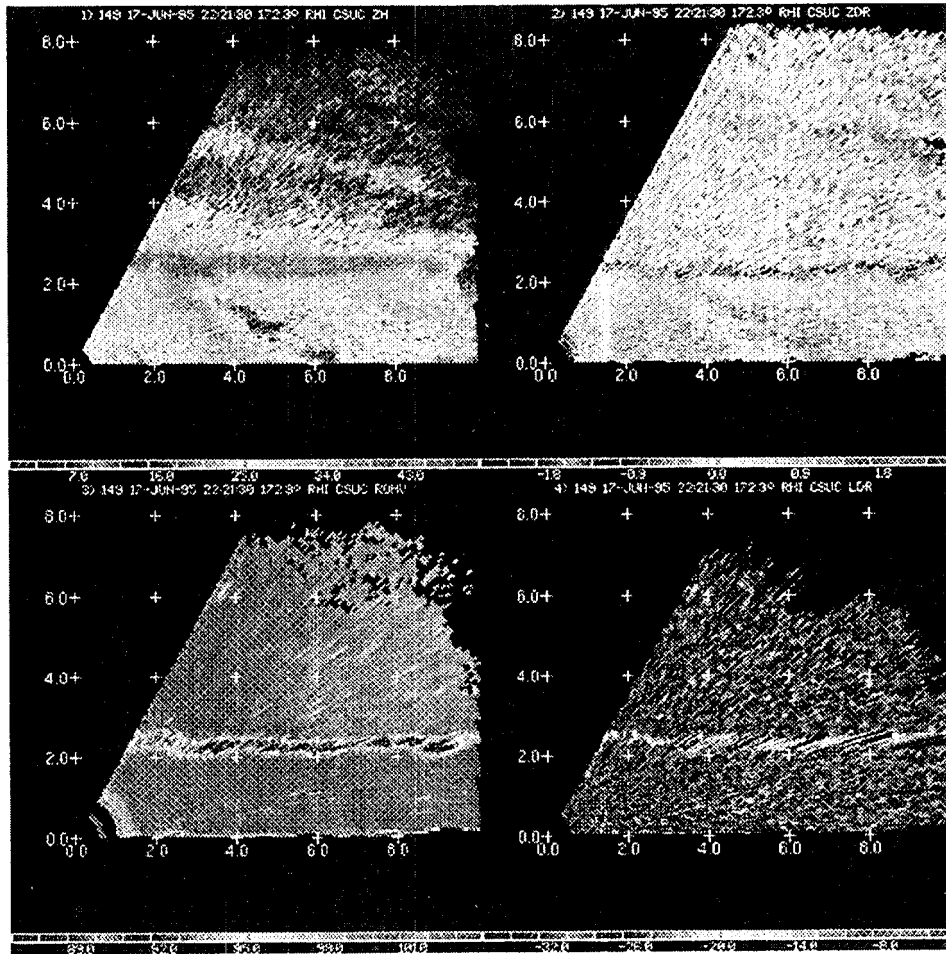


Figure 9: RHI scan for the June 18, 1995 stratiform case. The scan is taken along the radial of the ACTS propagation path. The CSU-APT elevation angle is 43° . The radar is located at the origin with the height given in km along the y-axis. Distance away from the radar along the 172° azimuthal angle is given in km along the x-axis. Horizontal reflectivity, Z_{HH} (dBZ), is shown in the upper left panel. Differential reflectivity, Z_{DR} (dB), is shown in the upper right panel. The cross correlation coefficient, ρ_{HV} (given as a percentage), is shown in the lower left panel. The linear depolarization ratio, LDR (dB), is shown in the lower right panel.

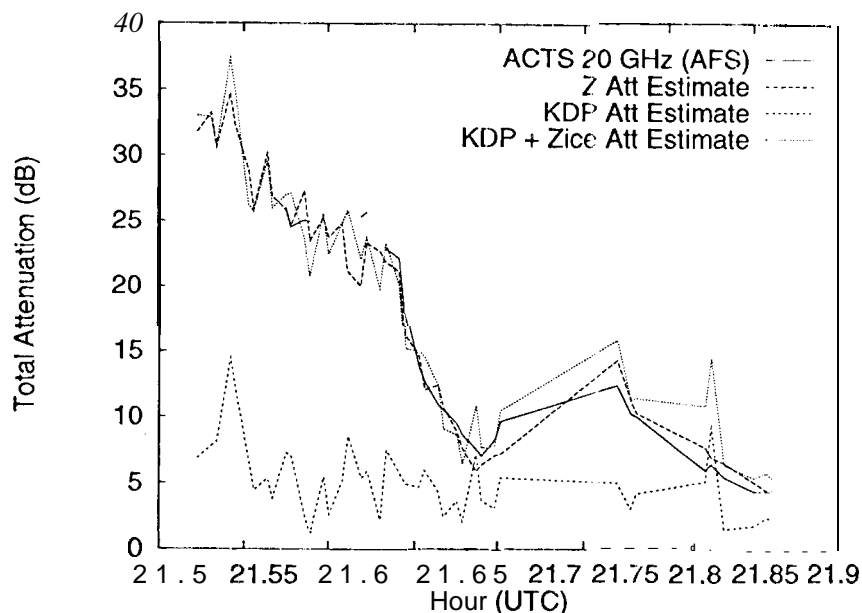


Figure 10: Comparison of measured CSU-APT attenuation and 20 GHz attenuation estimates derived from CSU-CHILL data.

CSU-CHILL derived estimates are within 1-2 dB of those measured by the CSU-APT. The attenuation estimates derived from *KDP* data alone grossly underestimated the attenuation caused by this event. This may be explained by examining Figure 11, a scatter plot of the APT measured 20 GHz attenuation versus the one way differential phase measured by the CSU-CHILL radar.

One way differential phase, Φ_{DP} , and its derivative *KDP* are only sensitive to the oblateness of a particle, therefore the difference seen between the maximum and minimum values of the fitted curve in Figure 11 is caused by the presence of various sizes of oblate rain drops present in the propagation path. If the hydrometers in the slant path were comprised of only raindrops the y-intercept of the fitted curve would be at zero; however, if the fitted curve is extended back to $\Phi_{DP} = 0$, the y-intercept is at 23.97 dB. This indicates that a large amount of attenuation was due to spherical, water coated ice particles. As indicated previously, there was indeed a region of mixed phase along the propagation path, however from Figure 11 and the fact that *KDP* data alone grossly underestimates the attenuation is an indication

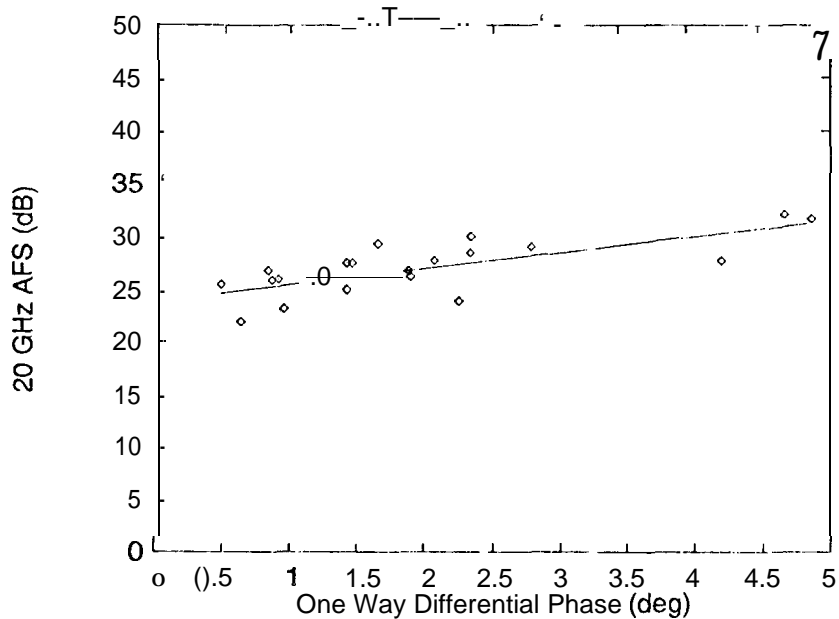


Figure 11: 20 GHz attenuation versus one way differential phase, for the June 20, 1994 convective case.

that water coated ice particles could have been present throughout a large part of the propagation path during this event.

Considering this to be the case, the next step is to determine the reflectivity due only to the water coated ice particles along the propagation path from the total reflectivity measured by the CSU-CHILL radar. This is done using the difference reflectivity, Z_{DP} , to determine the ice fraction content in the radar resolution volume at each 150 m increment along the propagation path. Once the ice fraction content is determined the reflectivity due only to the water coated ice particles, Z_{HH}^{ICE} , can be determined. The S-band reflectivity/Ka-band attenuation model is then used, with Z_{HH}^{ICE} as the input, to determine the attenuation at 20 and 27 GHz for the spherical, water coated hail particles. While the attenuation due to the oblate raindrops, Z_{HH}^{RAIN} , is computed using S-band KDP /Ka-band attenuation model.

The combined results are shown in Figure 10; while the attenuation estimates are still slightly underestimated for the most part, the CSU-CHILL derived attenuation estimates using KDP and Z_{HH}^{ICE} are within 1 to 2 dB of the the attenuation values obtained by the CSU-APT. The 27 GHz results

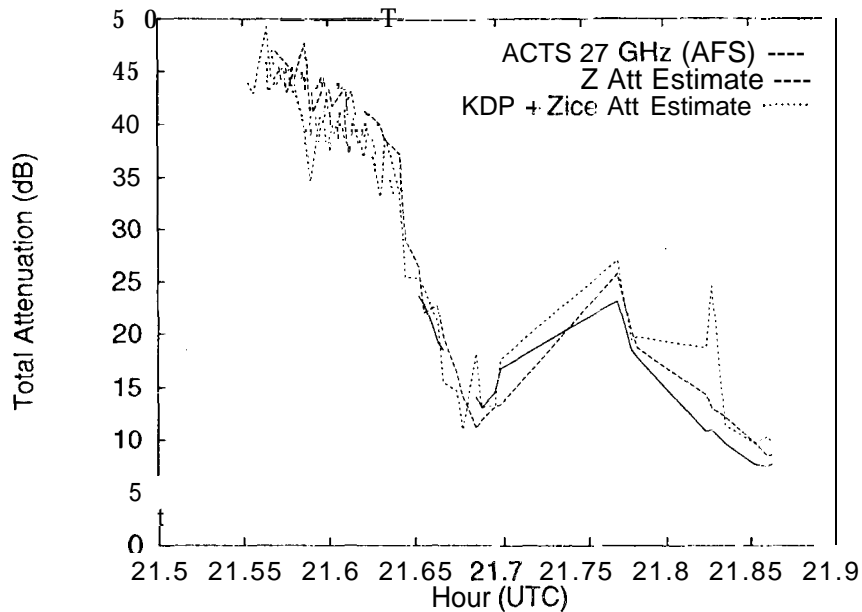


Figure 12: Comparison of measured CSU-APT attenuation and 27 GHz attenuation estimates derived from CSU-CHILL data.

are shown in Figure 12. The 27 GHz signal was interrupted for approximately 16 minutes during this event. At approximately 21:39 UTC, the 27 GHz signal was reacquired and as seen in Figure 12 the CHILL attenuation estimates are very close to the APT measured attenuation.

The results obtained by using the different polarimetric parameters available from the CHILL radar in this case is very encouraging. It is a good example of how the different parameters can be used to determine the nature of precipitation particles along the propagation path and predict Ka-band attenuation using S-band radar data.

Results for the May 18, 1995 convective case are shown in Figure 13. The attenuation estimates obtained from the S-band reflectivity data follow the trend of the beacon attenuation estimates. However, the radar attenuation estimates are off by a constant value at both frequencies, approximately 1.8 dB at 20 GHz and 3.0 dB at 27 GHz. This is also seen in the June 18, 1995 stratiform case, as shown in Figure 14. Here the reflectivity based attenuation estimates underestimate the APT attenuation estimates by 2 dB at 20 GHz and 3.3 dB at 27 GHz. Because of the frequency dependence of the underestimates it is unlikely that it can be attributed to a systematic error in the S-band radar constant, i.e., the absolute calibration of the radar. A simple increase in S-band reflectivity by a few dB would be inconsistent, not only with the frequency dependence, but also the difference in underestimates between the convective and stratiform portions of the same event (see Figure 14).

Underestimation of Ka-band attenuation levels from S-band radar data

May 18, 1995 Convective Case

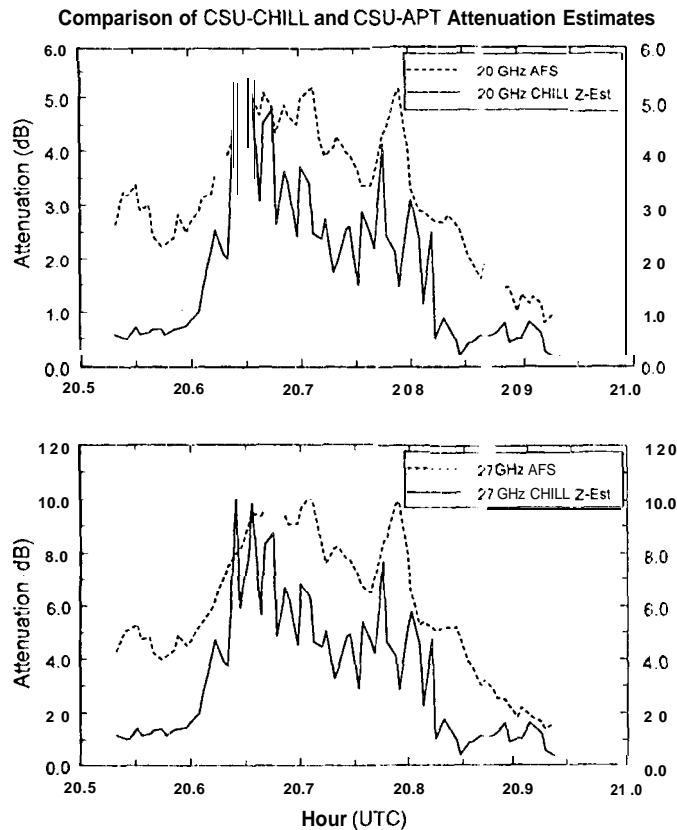


Figure 13: Comparison of measured CSU-APT attenuation at 20 and 27 GHz with attenuation estimates derived from CSU-CHILL S-band reflectivity data. For the May 18, 1995 convective case.

have been noted in previous studies [3], and the differences have been attributed to gaseous attenuation that is not measured at the S-band frequencies. However, in Colorado only 0.4 to 0.5 dB of attenuation can be attributed to the gaseous constituents. These values were determined by using radiometrically derived attenuation, as well as observations from radiosonde data taken from the Denver area. Gaseous attenuation and attenuation from cloud liquid water will contribute partially to the differences seen in the two cases described, but this contribution is small. A possible reason for the remaining difference is that water collecting on the antenna surface in the form of small droplets may cause appreciable amounts of attenuation. This possibility is examined by conducting a water spraying experiment. Under clear sky conditions, a garden hose was used to simulate the effect of rainfall on the antenna surface only, the feed horn surface only and both the antenna surface and feed horn surfaces simultaneously. The results of spraying the antenna surface alone are shown in Figure 15.

June 18, 1995 Stratiform Case

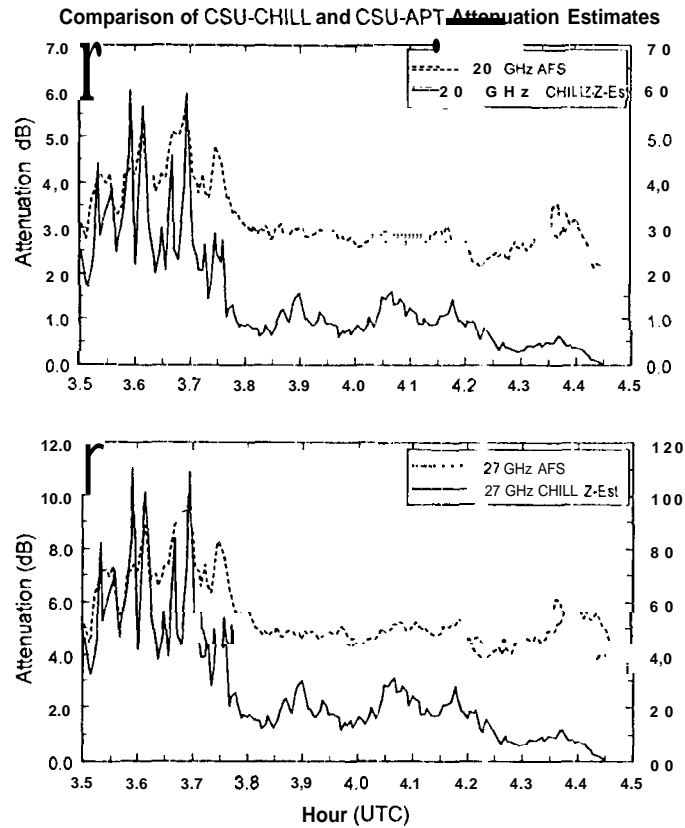


Figure 14: Comparison of measured CSU-APT attenuation at 20 and 27 GHz with attenuation estimates derived from CSU-CHILL S-band reflectivity data. For the June 18, 1995 stratiform case.

The antenna surface was continuously sprayed with water starting at 21:36:00 UTC and ending at 21:37:46 UTC. This is noted by the sustained peak attenuation in Figure 15. After the spraying had stopped there was a quick decrease in attenuation until 21:38:09. At this point, the attenuation continued to decrease but at a much slower rate. This measured attenuation is due to water standing on the antenna surface in the form of small droplets or beads. This beading effect will also occur during rain events and is dependent on the rain rate.

To check if the same type of frequency dependence is exhibited in the water spraying test as that seen in the differences between the attenuation estimates at 20 and 27 GHz shown in Figures 13 and 14, the instantaneous attenuation ratios were compared. The attenuation ratio for the water spraying test and for the June 18, 1995 stratiform case are shown in Figure 15. Once the spraying had stopped, the attenuation ratio between the June 18 event and the attenuation ratio computed from attenuation due to water

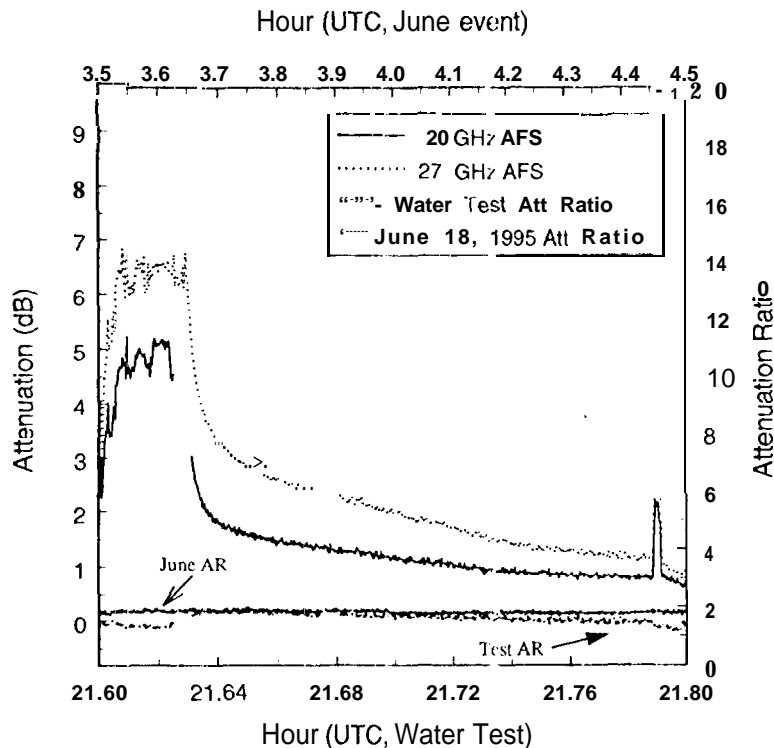


Figure 15: Water spray test results. Water was sprayed only on the antenna surface. Beacon attenuation for 20 and 27 GHz are shown, along with the instantaneous attenuation ratio for the two frequencies (20 GHz is the base frequency).

droplets on the antenna surface are identical for the most part. This gives a good indication that most of the difference seen between the attenuation estimates derived from S-band reflectivity data and CSU-APT attenuation estimates for the May 18 and June 18, 1995 events were due to water droplets that formed on the antenna surface.

The amount of attenuation caused by droplets forming on the antenna surface is dependent on the rain rate, wind direction and speed and the type of event, therefore it is not a systematic error that can be easily removed. While a hydrophobic solution was applied to the antenna surface to minimize this effect, water droplets still collect on the antenna surface. Several experiments were conducted by spraying the antenna surface with water. It was found that 1-5 dB of attenuation could occur at 27 GHz and 1-3 dB of attenuation at 20 GHz, just due to a water build-up on the antenna surface only. Results from spraying the feed horn surface show the beading effect does not occur with the same magnitude as seen on the antenna surface. In addition, the feed horn surface dries much quicker than the antenna surface. While it may be difficult to remove these effects, they do need to be taken into account for model development and in statistical analysis.

5 Conclusions

Due to the high demand for satellite communications, already overused portions of the frequency spectrum (C and Ku-bands) are becoming even more crowded. This necessitates looking at less crowded areas of the spectrum such as the Ka-band frequencies. To study satellite communications at these frequencies, NASA launched the Advanced Communications Technology Satellite (ACTS). The ACTS is an experimental satellite being used to conduct communication and propagation experiments using new Ka-band technology. At Ka-band, weather events can have an adverse affect on the signal being propagated through the atmosphere. Therefore, propagation effects at these frequencies must be studied. This report has outlined the research that has been conducted at CSU during the first two years to meet the ACTS experiment goals and further the understanding of K- band propagation effects.

The main goal of constructing an attenuation data base for the B2 climatic zone at K-band frequencies was met by maintaining a well calibrated ground propagation terminal and ensuring the integrity of the data collected and processed. Data were collected and preprocessed for the two year period of December 1, 1993 through November 30, 1995. A statistical analysis for the CSU-APT data was presented in Section 2 and Appendix A. The analysis was done on a monthly and annual basis.

An attenuation model was developed to relate S-band radar reflectivity to Ka-band attenuation. Several case studies were presented to illustrate the attenuation model. They included a very strong convective case, with known mixed phase, that occurred on June 20, 1994, a second, weaker convective event that occurred on May 18, 1995 and finally a stratiform event that occurred on June 18, 1995. Radar data, collected by the CSU - CHILL radar, for each of these events were used as inputs to the attenuation model. Very good results were obtained for each case.

Finally to conclude, the ACTS propagation experiment is an on-going experiment with two years of data collection completed, the third year in progress and the possibility of a fourth year. With the increased demand from industry to utilize the Ka-Band spectrum, the attenuation data being collected here, as well as at other sites, and its subsequent analysis will be invaluable for the field of satellite communications.